Optics Letters

Experimental characterization of quasiperiodic route to chaos in a VECSEL with SESAM

Camila Castillo-Pinto,[1,*] Marcel Clerc,[2] Heidi Ottevaere,[1] and Krassimir Panajotov[1,3]

[1]B-PHOT Brussels Photonics, Vrije Universiteit Brussel, Pleinlaan 2, Brussels, 1050, Belgium
[2]Departamento de Física and Millennium Institute for Research in Optics, Facultad de Ciencias Físicas y Matemáticas, Universidad de Chile, Santiago, Chile
[3]Institute of Solid State Physics, Bulgarian Academy of Sciences, Sofia, Bulgaria
*camila.de.jesus.castillo.pinto@vub.be

Received 29 September 2023; revised 10 November 2023; accepted 4 December 2023; posted 5 December 2023; published 8 January 2024

We analyze the temporal dynamics of an optically-pumped quantum well vertical external-cavity surface-emitting laser (VECSEL) with a Semiconductor Saturable Absorber Mirror (SESAM) using the time series obtained when varying the pump power. We unveil the quasiperiodic route to chaos in the system by characterizing the Fourier spectra, the attractors in phase space, and the Lyapunov exponents for each temporal behavior observed: periodicity, quasiperiodicity, and chaos. Thus, we provide a complete description of this experimental observation of the route to chaos in a VECSEL-SESAM system.

https://doi.org/10.1364/OL.507251

Nonlinear dynamics in semiconductor lasers has been widely studied from a fundamental point of view because of their widespread applications. Semiconductor lasers, such as edge-emitting lasers, distributed feedback lasers, vertical-cavity surface-emitting lasers (VCSELs), etc., are class B lasers because the gain medium polarization can be adiabatically eliminated in Maxwell–Bloch laser equations, leaving the electric optical field and population inversion as dynamical variables [1,2]. This means that the only dynamics they manifest is damped relaxation oscillations toward steady-state, and periodic, quasiperiodic, and chaotic dynamics cannot be observed [2–4]. Such complex dynamics, however, emerges when semiconductor lasers are subject to optical feedback [5–9], optical injection [1,10–14], external modulation [15,16], spin-flip carrier dynamics [17,18], incorporating coupled cavities [19,20] or saturable absorbers [21].

Recently, vertical external-cavity surface-emitting lasers (VECSELs) have attracted considerable interest as versatile and scalable high-power emitters [22] (for reviews see [23,24]). From a dynamical point of view, VECSELs are class A lasers because the photon lifetime inside the centimeter-long high-finesse external cavity is larger than the carrier lifetime [25]. Their nonlinear dynamics has been studied in [26,27] for the case of dual-wavelength operation and CW generation, periodic, quasiperiodic, and chaotic oscillations have been demonstrated. The external cavity provides great flexibility and VECSELs incorporating a saturable absorber mirror (SAM) are capable of generation *ps* and *fs* mode-locked pulses and serve as flexible frequency combs sources [28] (for reviews, see [29,30]). In [31], VECSELs with submonolayer quantum dot gain medium and semiconductor saturable absorber mirror (SESAM) are demonstrated experimentally to exhibit CW destabilization leading to chaotic pulsations. In the same year, another group mapped the different dynamical regimes of a 75-cm-long mode-locked VECSEL with SESAM, reporting the observation of CW emission, fundamental mode-locking, mode-locking of a few modes, double pulsing, and semi-stable 4th harmonic mode-locking [32]. However, none of the aforementioned investigations has experimentally reported or characterized the routes to chaos for VECSELs with SAMs. In a broader context, experimental investigation of the dynamical route to chaos holds significant importance, as it allows to explore the underlying mechanisms of chaos and nonlinear dynamics. This exploration is particularly relevant in cases where controlling or suppressing chaos becomes an objective. Furthermore, studying chaos from an experimental perspective contributes to the development of new techniques and methodologies for controlling and/or using chaotic behavior in practical applications, including message encryption and random number generation. In the specific case of VECSEL-SESAM systems, they serve as ideal platforms for such studies. The VECSEL-SESAM system's versatility and simplicity, together with its tunable parameters and controllable elements in free space, provide an ideal choice for investigating the dynamics of chaos in lasers and optical systems.

In this Letter, we analyze the temporal dynamics of an optically pumped quantum well VECSEL with SESAM using the time series obtained while varying the pump power. We unveil the quasiperiodic route to a chaotic regime in this system, characterizing the emergence of new frequencies, estimating its Lyapunov exponents and reconstructing the attractors in the phase space. To our knowledge, this Letter corresponds to the first experimental evidence and complete rigorous characterization of a quasiperiodic route to chaos in VECSELs with SESAM. Chaotic pulsations in a laser with a saturable absorber have been reported in a number of much earlier studies on CO_2 lasers with a saturable absorber [33–36]. However, the underlying dynamics of these lasers has been identified as Q switching behavior rather than mode-locking as in our case for VECSELs with a SESAM.

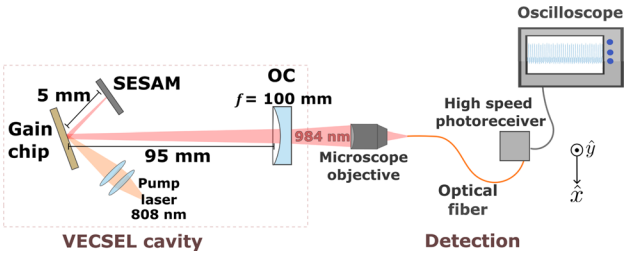

Fig. 1. Schematic representation of the VECSEL-SESAM setup. The laser cavity is assembled in V shape, with the gain chip as a folding mirror. The semiconductor saturable absorber mirror (SESAM) and Output Coupler (OC) act as ending mirrors. A microscope objective is focusing the light into a high-speed photodetector and sending it to an oscilloscope. The path of the output laser light is displayed in red.

Furthermore, the routes to chaos in CO_2 lasers are also of different nature: identified as homoclinic tangency to a periodic orbit (Shilnikov) route to chaos [34,36] and periodic doubling cascade [34].

The VECSEL V-shape cavity configuration and the detection setup are schematically shown in Fig. 1. The VECSEL consists of a semiconductor gain chip, a SESAM, and a dielectric mirror with a reflectivity of R=99.5% and curvature of 100 mm radius used as an output coupler (OC). The gain chip comprises 27 pairs of AlAs/GaAs quarter-wavelength layers forming a distributed Bragg reflector (DBR) deposited on top of a GaAs substrate. There are eight $In_{0.18}Ga_{0.82}As$ quantum wells (QWs), each approximately 8 nm thick. These QWs are separated by $\lambda/2$ GaAs barriers and, thus, positioned in antinode positions. A window layer made of $Al_{0.34}Ga_{0.66}As$ is grown to protect the carrier diffusion toward the wafer surface. Finally, a protective layer consisting of a 15-nm-thick GaAs cap is deposited to ensure the chip's longevity and optimal performance. A commercial SESAM, SAM-980-3-1ps from Batop Optoelectronics, with a high reflection band from 940 to 1000 nm, has been utilized. The laser cavity is assembled in a V-shape with the gain chip as a folding mirror, and the total cavity length is almost 100 mm, at which the resonator is close to becoming unstable. The temperature of the gain chip is stabilized at 9.5∘C by using a Peltier element attached to the submount with the gain chip, while the excess heat from the Peltier is removed by a water-cooled aluminum block. The gain chip is optically pumped with an 808 nm fiber-coupled diode laser at different pump powers. The maximum average output power achieved by the VECSEL with SESAM is 15 mW, emitting at 984.3 nm. In the detection branch, the output light is first directed to a microscope objective and then coupled into a multimode optical fiber. The light from the fiber is received by a high-speed photoreceiver (Newport New Focus 1554-B, 12 GHz bandwidth) connected to an oscilloscope (WavePro 804HD, 8 GHz of bandwidth and 20 GS/s sample rate), where the time series can be retrieved and analyzed.

The mode-locking behavior of our VECSEL-SESAM system has been fully characterized in [37]. For a pump power of 1.8 W the pulse width has been determined from the intensity autocorrelation traces to be about 2.3 *ps* and the repetition rate from the power spectrum to be about 1.45 GHz. By fixing the cavity length very close to the stability threshold of the resonator and increasing the pump power, P_{pump}, of the external laser, we observe a transition from a pulsed periodic behavior (from 225 mW to 250 mW of pump power) to a quasiperiodic regime (275 mW to 400 mW of pump power). By increasing P_{pump} above 425 mW, the quasiperiodic regime leads to chaotic behavior of the VECSEL with SESAM. The chaotic dynamics persists while pumping up to 950 mW. However, the lasing power starts to drop due to thermal rollover when the gain chip is pumped above 800 mW. The three top plots in Fig. 2 show the time series at three different pump powers, displaying the periodic, quasiperiodic, and chaotic behaviors mentioned above, respectively.

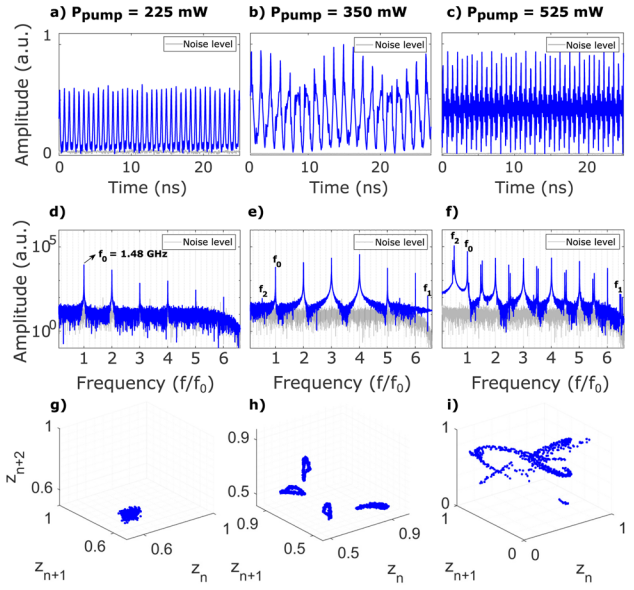

Fig. 2. Dynamical behavior of the VECSEL with SESAM. (a), (b), and (c) Time series of the VECSEL with SESAM output when the gain chip is pumped at different pump powers. There is a transition from periodic to quasiperiodic and chaos by increasing P_{pump}. For clarity, the time series have been rescaled to have values between 0 and 1. (d), (e) and (f) Fourier spectrum analysis of the time series when the gain chip of the VECSEL with SESAM is pumped at different pump powers. The frequencies in the Fourier spectra are normalized by the fundamental repetition rate associated with the total length of the cavity, f_0 = 1.48 GHz. (g), (h) and (i) Lorenz maps constructed by using consecutive peak amplitudes from the time series, named z_n, z_{n+1}, and z_{n+2}. The maps show the transition from a fixed point to the emergence of closed curves and from this to a scattered set of points. This transition occurs when increasing the pump power for the gain chip of the laser and corresponds to the quasiperiodic route to chaos from a periodic pulsed output.

To confirm the route to chaos, the Fourier spectra have been analyzed. For P_{pump} between 225 mW and 250 mW, the spectra show the fundamental repetition rate of the laser (f_0 = 1.48 GHz) and its harmonics ($2f_0$, $3f_0$, $4f_0$, $5f_0$, and $6f_0$), as presented in Fig. 2(a). For P_{pump} between 275 mW and 400 mW, the appearance of other peaks can be observed as shown in Fig. 2(b). In this case, two other frequencies have emerged: f_1 = 9.58 GHz and f_2 = 0.78 GHz; or in terms of the fundamental frequency: f_1 = 6.44 f_0 and f_2 = 0.52 f_0. Considering the presence of f_0, f_1, and f_2, we confirm the quasiperiodic behavior of the output power. For P_{pump} above 425 mW, multiple other peaks appear (which are linear combinations of the frequencies mentioned before), and some regions of the spectrum broaden, as seen in Fig. 2(c), which are key features of temporal chaos.

To characterize further the periodic, quasiperiodic, and chaotic behavior, we analyzed the Lorenz maps constructed

from tracking consecutive peak amplitudes, named z_n, at discrete time intervals. As expected for the periodic behavior, the map in Fig. 2(e) shows one fixed point. Rather than a single point, the data in Fig. 2(e) are spread in a small cloud, which is a consequence of noise in the system: at a pump power of P_{pump} = 225 mW, the output power is approximately 0.6 mW, and at this scale, noise becomes relevant during time series acquisition. In the quasiperiodic regime shown in Fig. 2(f), the Lorenz map exhibits closed curves associated with the intersection of the tori characterized by the different frequencies observed in the Fourier spectrum. Four closed curves are related to the highest peak in the Fourier spectrum, which is $4f_0$, meaning that the system is mostly ruled by four times the fundamental repetition rate. Finally, in the chaotic regime, the points are all scattered in the Lorenz map as depicted in Fig. 2(g).

While the Lorenz map simplifies the representation of the system's dynamics by reducing its continuous behavior to a discrete data set of points, a phase space reconstruction provides a tool to analyze the detailed and continuous dynamics, representing all the variables and possible states of the system. Reconstructing the phase space is possible using the time series and the time delay method [38,39]. The time delay method uses two important parameters: the delay parameter τ and the embedding dimension parameter *dim*. In brief, the embedding of the original time series $x(t)$ in the phase space means that consecutive values $x(t)$, $x(t+\tau)$, $x(t+2\tau)$, $\ldots x(t+(dim-1)\tau)$, are represented as a point in the phase space. Thus, by plotting the consecutive values for the complete data set of the time series, we reconstruct the phase space trajectories over which the system evolves in time, as shown in Fig. 3. The vertical axis is the original time series, and the horizontal axes represent the time series shifted in time by τ, 2τ, and 3τ.

For the periodic case [Fig. 3(a)], the attractor is shown as a closed orbit or limit cycle as expected, although the orbit is not completely clean due to noise. In Fig. 3(b), the quasiperiodic regime exhibits an attractor with well-defined and closed orbits. This attractor possesses one bigger orbit and three smaller orbits, related to the emergence of other frequencies in the system. Figure 3(c) displays the strange attractor for the case of deterministic chaos, with different shapes for different initial conditions.

By tracking the peak amplitude, z_n, of the time series as a function of P_{pump}, a bifurcation diagram is obtained and shown in Fig. 4(a). The transitions from periodic to quasiperiodic behavior following the chaotic states are distinguished in this figure. In contrast to the relatively constant peak amplitude observed in periodic or quasiperiodic regimes, chaotic states display a broad range of peak amplitudes due to the existence of a strange finite attractor in the phase space that the system fully explores over time. As shown in Fig. 4(a), for pump powers up to approximately 400mW, the system dynamics is periodic, i.e., the time traces of the peak amplitude exhibit one or two amplitudes, each associated with its respective error bar that is accounting for the system noise. However, for pump powers above 400mW the system is chaotic, i.e. the peak amplitude time traces form continuous vertical lines covering certain continuous ranges of amplitudes. For further confirmation of temporal chaos, the Lyapunov exponents are rigorously calculated for each pump power. The method to calculate Lyapunov exponents from a time series consists of considering two points of similar amplitude at different times that represent two nearby initial conditions in phase space. Thus, the difference between them is tracked as time evolves [40]. The estimation of Lyapunov exponents is carried

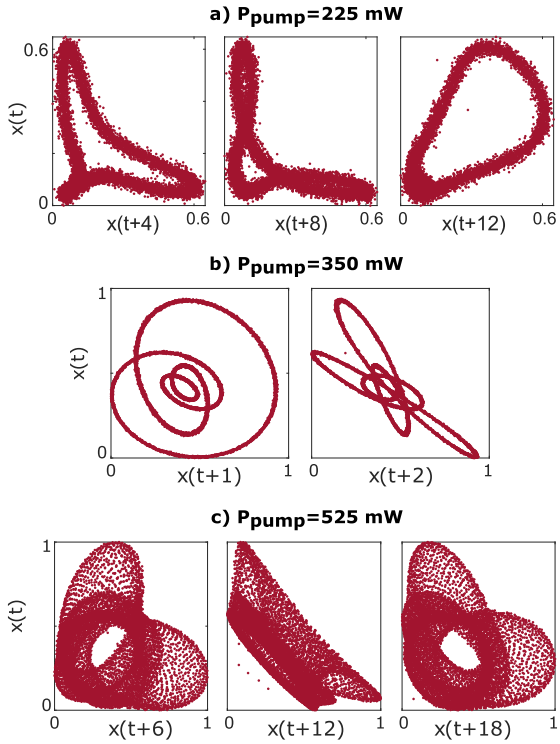

Fig. 3. Reconstructed phase space, based on the time delay method. For the three cases, the time delay τ is estimated using the average mutual information algorithm, and the embedding dimension *dim* is estimated using the false nearest neighbor algorithm. (a) $\tau = 4$, $dim = 4$. (b) $\tau = 1$, $dim = 3$. (c) $\tau = 6$, $dim = 4$.

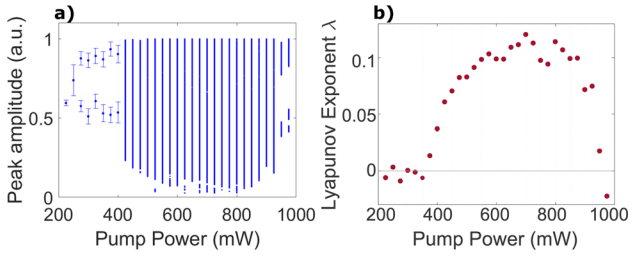

Fig. 4. (a) Bifurcation diagram constructed from the amplitude of the peaks as a function of P_{pump}. (b) Lyapunov exponents for different P_{pump}.

out for different P_{pump} and the results are shown in Fig. 4(b), where we observe once more the chaotic region of the system characterized by positive Lyapunov exponents for P_{pump} between 400 mW and 950 mW.

In summary, we present experimental evidence and characterization of the route to deterministic chaos in a VECSEL with SESAM system based on the analysis of time series. We show the emergence of new frequencies and the consequent broadening of the spectrum of the system that indicates a quasiperiodic route to chaos when increasing the pump power of the VECSEL. We construct the Lorenz maps for each of these behaviors, showing the transition from a fixed point (periodic) to cross sections of tori (quasiperiodic), followed by a strange attractor shape that suggests the loss of periodicity and the chaotic nature of the attractor. By using the time delay method, we reconstruct the attractors for each dynamical regime, displaying

the strange attractor for temporal chaos. Furthermore, we obtain the bifurcation diagram by tracking the peak amplitudes as a function of pump power. Finally, we calculate the Lyapunov exponents as a function of the pump power. Both the bifurcation diagram and the Lyapunov exponents confirm beyond doubt the deterministic temporal chaos observed in the output light from VECSELs with SESAM. It is important to notice that the threshold values for the different transitions shown in the bifurcation diagram depend directly on the temperature of the gain chip. Moreover, the impact of the temperature and the optical pump power on the laser dynamics are related. As the optical pump power increases, the temperature of the gain medium also rises. Higher temperatures change the characteristics of the gain medium, such as its spectral response and saturation level. This change in the gain due to temperature can influence the laser's transition from periodic behavior to more complex regimes, such as chaos. Furthermore, by maintaining the gain medium at lower temperatures, the threshold for transition to more complex behaviors decreases, making it easier to achieve these complex states. These studies offer valuable insights into the intricate temporal dynamics of VECSELs when combined with SESAM. Beyond enhancing our understanding of these systems, the simplicity and versatility of such cavities make them ideal platforms for investigating a wide range of chaos-related phenomena, including synchronization and chaos control, or for further exploration of practical applications such as message encryption and random number generation in a straightforward manner.

Funding. Fonds Wetenschappelijk Onderzoek (G0E5819N); Fondo Nacional de Desarrollo Científico y Tecnológico (1210353); Millennium Institute for Research in Optics (MIRO); Methusalem and Hercules Foundations; Vrije Universiteit Brussel (OZR).

Disclosures. The authors declare no conflicts of interest.

Data availability. Data underlying the results presented in this paper are not publicly available at this time but may be obtained from the authors upon reasonable request.

REFERENCES

1. J. R. Tredicce, F. T. Arecchi, G. L. Lippi, *et al.*, J. Opt. Soc. Am. B **2**, 173 (1985).
2. J. Ohtsubo, *Semiconductor Lasers. Stability, Instability and Chaos*, Vol. 111 (Springer, 2013).
3. P. Berge, P. Y. C. Vidal, D. Ruelle, *et al.*, *Order within Chaos: Towards a Deterministic Approach to Turbulence* (Wiley, 1984).
4. P. Mandel, *Theoretical Problems in Cavity Nonlinear Optics* (Cambridge Studies in Modern Optics, 1942).
5. K. Mukai and K. Otsuka, Phys. Rev. Lett. **55**, 1711 (1985).
6. D. Lenstra, B. H. Verbeek, and J. D. Boef, IEEE J. Quantum Electron. **21**, 674 (1985).
7. J. Mork, J. Mark, and B. Tromborg, Phys. Rev. Lett. **65**, 1999 (1990).
8. J. Ohtsubo, Opt. Rev. **6**, 1 (1999).
9. A. Tabaka, K. Panajotov, I. Veretennicoff, *et al.*, Phys. Rev. E **70**, 036211 (2004).
10. J. Sacher, D. Baums, P. Panknin, *et al.*, Phys. Rev. A **45**, 1893 (1992).
11. V. Annovazzi-Lodi, IEEE J. Quantum Electron. **30**, 1537 (1994).
12. T. B. Simpson, J. M. Liu, A. Gavrielides, *et al.*, Appl. Phys. Lett. **64**, 3539 (1994).
13. S. Wieczorek, B. Krauskopf, and D. Lenstra, Opt. Commun. **172**, 279 (1999).
14. J. Buesa, I. Gatare, K. Panajotov, *et al.*, IEEE J. Quantum Electron. **42**, 198 (2006).
15. Y. Hori, H. Serizawa, and H. Sato, J. Opt. Soc. Am. B **5**, 1128 (1988).
16. A. Valle, M. Sciamanna, and K. Panajotov, IEEE J. Quantum Electron. **44**, 136 (2008).
17. M. Virte, M. Sciamanna, and K. Panajotov, Opt. Lett. **41**, 4492 (2016).
18. T. R. Raddo, K. Panajotov, B. H. Borges, *et al.*, Sci. Rep. **7**, 14032 (2017).
19. H. Erzgraber, S. Wieczorek, and B. Krauskopf, Phys. Rev. E **78**, 066201 (2008).
20. M. Ozaki, H. Someya, T. Mihara, *et al.*, Phys. Rev. E **79**, 026210 (2009).
21. H. Kawaguchi, Appl. Phys. Lett. **45**, 1264 (1984).
22. M. Kuznetsov, F. Hakimi, R. Sprague, *et al.*, IEEE Photonics Technol. Lett. **9**, 1063 (1997).
23. A. C. Tropper, H. D. Foreman, A. Garnache, *et al.*, J. Phys. D: Appl. Phys. **37**, R75 (2004).
24. M. Guina, A. Rantamäki, and A. Härkönen, J. Phys. D: Appl. Phys. **50**, 383001 (2017).
25. G. Baili, L. Morvan, M. Alouini, *et al.*, Opt. Lett. **34**, 3421 (2009).
26. Y. A. Morozov, A. I. Konyukhov, L. A. Kochkurov, *et al.*, Quantum Electron. **41**, 1040 (2011).
27. M. Y. Morozov, Y. A. Morozov, and I. V. Krasnikova, J. Commun. Technol. Electron. **55**, 1162 (2010).
28. S. Hoogland, S. Dhanjal, A. C. Tropper, *et al.*, IEEE Photonics Technol. Lett. **12**, 1135 (2000).
29. U. Keller and A. C. Tropper, Phys. Rep. **429**, 67 (2006).
30. B. W. Tilma, M. Mangold, C. A. Zaugg, *et al.*, Light: Sci. Appl. **4**, e310 (2015).
31. C. G. Alfieri, D. Waldburger, J. Nürnberg, *et al.*, Phys. Rev. Appl. **10**, 044015 (2018).
32. T. Malica, J. Lin, T. Ackemann, *et al.*, Opt. Express **26**, 16624 (2018).
33. D. Dangoisse, A. Bekkali, F. Papoff, *et al.*, Europhys. Lett. **6**, 335 (1988).
34. D. Hennequin, F. de Tomasi, B. Zambon, *et al.*, Phys. Rev. A **37**, 2243 (1988).
35. M. Tachikawa, F.-L. Hong, K. Tanii, *et al.*, Phys. Rev. Lett. **60**, 2266 (1988).
36. H. L. D. de S. Cavalcante and J. R. R. Leite, Chaos **18**, 023107 (2008).
37. C. Castillo-Pinto, A. Broda, I. Sankowska, *et al.*, Opt. Express **30**, 47497 (2022).
38. MATLAB, "Phase space reconstruction. convert observed time series to state vectors," https://fr.mathworks.com/help/predmaint/ref/phasespacereconstruction.html.
39. H. D. I. Abarbanel, *Analysis of Observed Chaotic Data* (Springer, 1996).
40. A. Wolf, J. B. Swift, H. L. Swinney, *et al.*, Phys. D **16**, 285 (1985).